https://doi.org/10.1016/j.ijfatigue.2019.04.017

Brittle coating effects on fatigue cracks behavior in Ti alloys

Yanyun Bai [a], Yeting Xi [a], Kewei Gao [a], Huisheng Yang [a], Xiaolu Pang [a*], Xusheng Yang [b], Alex A. Volinsky [c*]

[a] *School of Materials Science and Engineering, University of Science and Technology Beijing, Beijing 100083, China*

[b] *Department of Industrial and Systems Engineering, The Hong Kong Polytechnic University, Hung Hom, Kowloon, Hong Kong, China*

[c] *Department of Mechanical Engineering, University of South Florida, Tampa, FL 33620, USA*

Abstract

In order to study the coating effects on fatigue crack initiation mechanism in Ti-alloys, two types of brittle coatings, CrAlN and TiN, were deposited on the surface of TC4 titanium alloy by physical vapor deposition. The tension-tension fatigue tests and the in-situ observations of fatigue crack morphology were performed to study the coating effects on the fatigue crack initiation and propagation in the Ti-6Al-4V alloy. It was found that the 510-530 MPa TC4 fatigue limit is reduced to 315-330 MPa due to the CrAlN coating. The brittle coatings impeded the deformation of the TC4 samples at the beginning stage of fatigue tests, while coating cracking promoted the elongation of the tested samples. Fatigue crack was found to be initiated in the brittle coatings and propagated to the coating-substrate interface, inducing micro-damage of the substrate surface. The fracture surface of coated and uncoated samples was cardinally different, and the formation of non-propagating fatigue cracks was also observed. The coating cracking-induced low cyclic stress substrate damage model was proposed. This study should be of significance

*Corresponding authors: Xiaolu Pang, tel: (+86)010-82376048, fax: (+86)010-82376048, email: pangxl@mater.ustb.edu.cn, Beijing Advanced Innovation Center for Materials Genome Engineering, Beijing 100083, China, 30 Xueyuan Road, Haidian District, Beijing 100083, China; Alex A. Volinsky, volinsky@usf.edu

for the coating improvement and provides a theoretical basis for improving fatigue properties of coating materials.

Keywords: Surface coatings; fatigue crack; initiation mechanism; Ti alloys.

1. Introduction

Due to the high strength/weight ratio, adequate corrosion resistance [1] and biocompatibility, Ti alloys are promising materials for cutting tools, automotive industry, medical and aerospace applications. However, poor wear resistance restricts Ti alloys applications, and hard coatings are considered to be a convenient and effective surface strengthening technique for Ti alloys. Structural compounds, turbines and numerous other components of aerospace systems are cyclically loaded and subjected to more than 10 million cycles until they are replaced, so materials are subjected to high cycle fatigue (HCF, $10^5 < N < 10^7$) and even very high cycle fatigue (VHCF, $N > 10^7$) regimes [2]. According to the service condition of aerospace parts, such as aircraft engine compressor blades, the effects of coatings on fatigue properties have attracted a lot of researchers' attention.

The change of fatigue life was considered to depend on the residual stress [3] and the hardness of the hard coatings and the substrate [4], and also adhesion between the coating and the substrate [5]. Saini et al. [3] illustrated that the WC/C coating led to 7% gain in endurance limit of the SAE8629 steel, which was attributed to the presence of a large residual compressive stress in the coated specimens. Puchi-Cabrera et al. [6] reported that diamond-like carbon (DLC) coatings elevated the fatigue limit of ductile substrates in both air and 3 wt.% NaCl solution. However, there are conflicting reports. Costa et al. [7] studied CrN, DLC and TiN coatings on the Ti-6Al-4V substrate and pointed out that all the

three hard coatings decreased the fatigue limit of Ti-6Al-4V. Midori et al. [8] pointed out that TiN coating on Ti alloy reduced fatigue strength of the substrate due to the small voids in the coating acting as stress concentration points, which were regarded as fatigue crack initiation sites.

The conflicting research results illustrate that the brittle coating effects on fatigue behavior of ductile substrates are not clear yet. The key aspect of the scientific significance is to understand the mechanism of fatigue crack initiation and early growth during the fatigue process. For materials with nonmetallic inclusions or strengthening-phase particles, such as some high strength steels, cracks are prone to initiate at specimen subsurface or interior with a distinct feature of "fish-eye" embracing fine-granular-area (FGA) originated from an inclusion [9-12]. As reported in the literature [13], titanium alloy is a typical material that shows subsurface non-defect crack origins (SNDFCO) under cyclic uniaxial loading conditions, which means the fatigue crack initiated at the subsurface non-defect area or the matrix that is not associated with pre-existing defects, and SNDFCO were also observed in some austenitic stainless steels [14, 15]. The reason is considered to be microstructure inhomogeneity [16, 17]. Researchers pointed out that the size and morphology of SNDFCO strongly depend on the applied stress [18], and the crack extension rate in the rough area is between 10^{-11} and 10^{-13} m/cycle [19].

Although the study on metal fatigue crack initiation mechanism has drawn a lot of attention in the last few decades, and many achievements had been made [20-24], the fatigue crack initiation mechanism of brittle coating-ductile substrate system is not clear. Thus, the aim of this paper is to experimentally study fatigue behavior of brittle film coated Ti alloy under low stress level cyclic loading conditions, and to investigate the coatings influence on fatigue crack initiation in materials without metallurgical defects, such as inclusions or pores, which can act as crack initiation sources in the fatigue process.

The study of the influence of brittle films on the fatigue properties and fatigue crack initiation mechanisms in ductile substrates is helpful to evaluate the fatigue life of coating materials. It is of great significance for the film improvement and provides a theoretical basis for improving fatigue properties of coated materials.

2. Materials preparation and experimental procedure

The test material in this research is Ti-6Al-4V (TC4), with the following chemical composition in wt.%: 6.2 Al, 4.1 V, 0.04 Fe, 0.015 C, 0.018 N, 0.13 O, 0.001 H, and Ti balance. The microstructure is lamellar consisting of α+β phases and the grain size is about 200 μm. The yield and tensile strength of TC4 are 860 MPa and 967 MPa, respectively. Two kinds of coatings were studied, including TiN and CrAlN. All coatings were deposited in an industrial setting and all deposition processes were finished in the factory. The thickness of the CrAlN coatings is 4.5 μm and 9 μm, respectively (marked as CrAlN and CrAlN×2), and 10 μm for TiN. The coatings surface hardness and elastic modulus were obtained by nanoindentation tests (Nano Indenter XP, unloading method, the maximum displacement into surface was controlled to be less than 1/10 of the film thickness) and the results are shown in **Fig. 1**.

Tension-tension fatigue tests were conducted using the electrodynamic test system (Acumen, MTS) in high cycle fatigue region at a relatively low frequency of 60 Hz, in order to observe the crack initiation and propagation behavior, and the stress ratio was R=0.1. Fatigue tests were divided into two groups. (1) The tests stopped automatically when the specimen fracture happened, the S-N data (applied maximum stress-number of cycles to failure) were recorded and the fracture surface was studied to discuss the coating effect on fatigue life and fatigue crack initiation mechanism. (2) Optical microscopy was used to in-situ observe fatigue crack growth during fatigue tests, and the tests were stopped immediately when the cracks propagated to about 500 μm length, in order to observe the

cross section of crack tips to study the influence of coatings on crack propagation path and substrate plastic deformation around the crack tips.

The dimensions of fatigue specimens are shown in **Fig. 2**, where the thickness ranged from 0.5 to 0.7 mm due to different polishing losses in the specimens' preparation process. The specimen's maximum displacement during tension-tension fatigue test was recorded automatically by the control system. Field emission scanning electron microscopy (FESEM, Zeiss Auriga) was used to examine fatigue fracture surfaces and the micro-cracks around the crack tip in the cross-section perpendicular to the loading direction.

3. Results and Discussion

3.1 Fatigue life

Fig. 3 shows the tension-tension fatigue test results of the coated TC4 samples. The fatigue limit is regarded as the applied maximum stress value when the fatigue life equals 10^7 cycles ($N=10^7$) [25]. The following information can be obtained from **Fig. 3**:

1. The fatigue limit of TC4 was between 510 and 530 MPa;
2. The coatings decreased the TC4 fatigue life significantly, and the fatigue limit of the CrAlN coated sample was between 315 and 330 MPa;
3. The fatigue life of three kinds of coated samples was similar at 560 MPa;
4. When the applied stress was 350 MPa, the fatigue life was in the following order: N_f (TiN) < N_f (CrAlN×2) < N_f (CrAlN);
5. The CrAlN coated samples failure did not happen at 300 MPa, and N_f (TiN) was about 10^5.

According to the actual test conditions, it is very difficult to get the applied maximum

stress under which the fatigue life of the sample is exactly 10^7, so we specify in the experiment that when the difference between the applied maximum stress induces and does not induce the fatigue fracture of the sample is less than 5% of the stress value, then the stress range is regarded as the fatigue limit range.

3.2 Coating effects on elongation

Fig. 4 presents optical images of the fatigue crack surface morphology and displacement-number of cycles relationship (D-N curves) of TC4 and coated samples during fatigue tests. The displacement represents the elongation of the specimens during fatigue tests and the fatigue tests were stopped immediately when the cracks propagated to about 500 μm length. The loading direction was along the horizontal direction of the images and vertical with respect to the cracks in the figure. As seen in **Fig. 4(a)**, TC4 had a large number of slip steps around the crack initiation area (top area of the specimen), propagation path and the crack tip. Intense plastic deformation around the crack tip was induced by stress concentration during the crack propagation process. Based on the D-N curve, the elongation of TC4 first decreased and then increased during the fatigue process, until fracture happened, which indicated that the strain hardening happened at the beginning of the fatigue test due to plastic deformation of the primary α phase [16], and the deformation process of the TC4 sample was uniform during the whole fatigue process. On the contrary, there was no distinct plastic deformation around the crack tip or visible slip steps around the crack initiation area and propagation path on the surface of coated samples (**Fig. 4(b)**, **(c)** and **(d)**), but a few micro-cracks of coatings perpendicular to the loading direction appeared around the main fatigue cracks. The main fatigue cracks were straight and of lightning-like shape, which indicated that the fatigue cracks propagated along the coating cracking path, or in another word, the cracking of coatings influenced the propagation path of the fatigue cracks. At the same time, the D-N curves of the coated

samples had several steps during the fatigue tests, which indicated that the deformation process of the samples was not uniform.

Fig. 5 shows the schematic diagram of the deformation mechanism of TC4 and coated TC4 materials, where the loading direction is horizontal. For TC4 material during the cyclic loading process, as shown in **Fig. 5(a)**, **(b)** and **(c)**, dislocations pile-up at the phase boundary of the primary α and laminar β phases at the subsurface of TC4, due to the difference in deformation capacity [16]. Under the cyclic loading, the dislocations cross the grain boundary and pile-up at the specimen's surface, inducing the glide step appearing on the specimen's surface. This glide step can cause stress concentration during the loading process and finally act as the fatigue crack initiation point of the uncoated specimen. The elongation Δl of the TC4 specimen due to sliding is also pointed out in **Fig. 5(b)**.

There are many reports [26-28] showing that in the process of plastic deformation, a hard coating can inhibit the dislocations escape from the substrate crystal surface, because the strain energy of dislocations in hard coatings is higher than in the ductile substrates, preventing plastic deformation of the substrate [29]. Under the effect of hard coatings, although dislocations can pile-up at the surface of the TC4 substrate, the sliding deformation of the material was inhibited, as shown in **Fig. 5(d)**. However, when the elastic elongation of the substrate exceeds the deformation capacity of the surface brittle coating, the coating cracking will happen and act as the fatigue crack initiation origin of the specimen. The fatigue crack opening displacement is regarded as the plastic elongation of the coated specimen, as denoted as Δl' in Fig. 5(e).

Based on the above instructions, for the coated specimen at the early stage of fatigue tests, strain hardening happened and the coatings prevented deformation of the samples, which was embodied in the lowest points (red line in the graph) of the coated samples' curves being lower than the TC4 sample's, as shown in **Fig. 4(b)**, **(c)** and **(d)**. Then the

elongation curve increased and remained at a steady value range several times, due to the inhibiting effect of hard coatings on plastic deformation (sliding) of the substrate. After the coating fatigue cracking happened (regarded as the fatigue crack of the specimen), severe stress concentration occurred at the crack tip, and the plastic deformation of the specimen increased immediately, and the specimen's elongation is regarded as the opening displacement of the fatigue crack. Thus, the elongation curve of the coated specimen shows the "step" shape.

Summing up the above discussion, the existence of hard coatings prevented the plastic deformation of TC4 samples before the coating cracking happened, and had a positive effect on sample plastic deformation (or cracking) after coating cracking happened.

3.3 Fatigue crack cross section

The crack tip cross-section morphology of the CrAlN coated sample is shown in **Fig. 6**, where the loading direction is horizontal as shown in **Fig. 6(a)**, and the tested conditions were σ_{max}=500 MPa, R=0.1, f=40 Hz, and the fatigue test was stopped manually when the crack propagated to about 500 μm length. The crack tip cross-section sampling location is shown in **Fig. 6(c)**. As seen in **Fig. 6(a)**, the propagation process of fatigue cracks can be divided into several stages. The fatigue cracks first propagated along the maximum shear stress direction, and in this stage most of the cracks became non-propagating fatigue cracks, so only one could go into the next stage and became the main fatigue crack, which lead to the final failure. Then the main fatigue crack propagated perpendicular to the loading direction, and created fatigue bands on the fracture surface. Finally, the shear lip formed until instant fracture of the samples happened.

Fig. 6(b) shows the typical non-propagating fatigue cracks observed near the main crack. The mechanism of whether a micro-crack continues propagating or becomes a non-propagating fatigue crack is not clearly described in the literature and will be

discussed later based on the coating cracking-induced low cyclic stress substrate damage model.

4. Coating cracking-induced low cyclic stress substrate damage model

It's generally recognized that the fatigue crack initiation process consumes about 90% of the fatigue life for components without metallurgical defects (such as inclusions), and the percentage can sometimes reach up to 95% [9, 30]. Thus, the negative influence of coatings on the fatigue life comes down to the accelerating effect on fatigue crack initiation process.

As reported in the literature [13, 18], titanium alloy is a typical material that shows subsurface non-defect fatigue crack origins (SNDFCO), which is characterized by the fish eye structure, and the center of the fatigue crack origin is a circular rough area surrounded by a more smooth area, as shown in **Fig. 7(a)**. Judging from the crack propagation trace, the fatigue crack of TC4 propagated from the subsurface of the specimen to the surface and into the matrix material, and then induced the final failure of the specimen.

The stress intensity factor (SIF) at the front of SNDFCO can be calculated using the following equation [9, 31]:

$$\Delta K = 0.5\sigma_{max}\sqrt{\pi\sqrt{area}} \quad (1)$$

where σ_{max} is the maximum applied stress and *area* is the equivalent area of the SNDFCO.

4.1. Coating effect on fatigue crack initiation mechanism in TC4

It should be noted that the crack initiation source on the fracture surface of coated samples (**Fig. 7(b), (c)** and **(d)**) differs a lot from the uncoated TC4. As shown in **Fig. 7(b)**, the darker part on the left side of the fatigue fracture is the CrAlN coating. Brittle fracture happened in the coating, and there was obvious crack propagation trace from the coating-substrate interface into the matrix material. There was no typical circular fish eye

fatigue crack initiation area on the fatigue fracture surface of the coated samples. Also, there were more than one fatigue crack initiation areas on the fracture surface, as pointed out and magnified in **Fig. 7(b), (c) and (d)**. The crack propagation trace from the interface into the bulk material indicates that the crack initiated in the coating is different from TC4 (**Fig. 7(a)**), which initiated at the subsurface of the substrate.

Fig. 8 is the SEM image of the fatigue crack initiation process in coated TC4, the loading direction is horizontal as shown in **Fig. 8(a)**. As shown in **Fig. 8(a),** the coating fatigue crack initiated at the middle of the hard coating. **Fig. 8(b)** shows the substrate surface damage (micro-cracks) induced by coating cracking, and under the cyclic loading, the substrate surface damage (micro-cracks) will propagate as shown in **Fig. 8(c)**, **Fig. 8(d)** is the cross-section SEM image of the main fatigue crack, which will lead to the final fatigue fracture of the material.

In order to clearly identify the fatigue crack initiation mechanism in coated TC4, the fatigue crack cross-sections were studied carefully before and after the fatigue crack initiation. The coating cracking-induced low cyclic stress substrate damage model (CCILCSSD) was proposed. Fatigue cracking initiated at the middle area of the hard coating [32] at the early stage of the fatigue process, and propagated to the coating surface and coating-substrate interface. The fast-running crack caused the surface micro-damage of the substrate material, where under the cyclic loading, the micro-damage developed into small fatigue cracks, and most of them became non-propagating fatigue cracks, and only one of them could keep propagating and finally induced the fatigue fracture of the specimen.

From the energy standpoint, the premise of coating crack initiation and propagation is the increased surface energy equal to the released internal energy. According to the literature [33], the total energy can be determined by the following expression:

$$E_{total} = -\frac{\sigma_m^2}{2E'} wah + 2\gamma aw \quad (2)$$

Here, σ_m, E', w, a and h are applied stress, elastic modulus, width and length of the crack and coating thickness, respectively, and γ is the surface energy per unit area of the crack. When the crack initiates at h_c, one can get

$$\frac{dE_{total}}{da}\Big|_{h=h_c} = -\frac{\sigma_c^2}{2E'}\mathrm{wh} + 2\gamma\mathrm{w} = 0 \quad (3)$$

One can obtain the critical stress, σ_c:

$$\sigma_c = \sqrt{\frac{4E'\gamma}{h_c}} \quad (4)$$

Since $4E'\gamma = K_{IC}$,

$$\sigma_c = \sqrt{\frac{K_{IC}}{h_c}} \quad (5)$$

Since the critical stress intensity, K_{IC}, is constant for a specific material, the critical applied stress is determined only by the mechanical properties of the coating. Since the mechanical properties and thickness of the CrAlN and TiN coatings deposited on the TC4 surface are similar in this study, the fatigue life of the coated samples is similar too.

According to the Miner's linear damage accumulative theory, the damage *D* of the material per one cycle is defined as $1/N_f$, so the distribution of the damage along the crack growth direction in the cyclic plastic zone can be described as [33]:

$$\mathrm{D}(\mathrm{r}+\rho_c) = 2\left(\frac{\sigma_{yc}}{E\varepsilon_f'}\right)^{-\frac{1}{d}}\left(\frac{r_c}{\mathrm{r}+\rho_c}\right)^{1/(d+dn')} \quad (6)$$

Combined with the above discussion, when the fatigue crack extends from the coating to the substrate surface, the crack velocity will remain the same, and since *E* of the brittle coatings is larger than the ductile substrate, the *D* value of the coating crack is larger than

the crack extension in the substrate material. Thus, as shown schematically in **Fig. 9(a)**, when the surface crack propagates to the interface of the coating and the substrate, and a micro-crack of the substrate induced by the fast-running film crack appears on the substrate surface [32], the mechanical properties of the crack tip, point C, are the same as the substrate, as seen in **Fig. 9(b)**. The crack velocity of the point C in **Fig. 9(b)** is lower than points B and A, the crack tip becomes blunt and the crack in the coating propagates rapidly, until the coating crack extends to the entire surface of the specimen.

This is the reason for the formation of the coating cracks around the main fatigue crack in **Fig. 4 (b)**, **(c)** and **(d)**. Because of the damage caused by the coating cracks, the fatigue crack tends to propagate along the substrate surface damage direction, so the main fatigue crack has the lightning shape.

4.2. The formation of non-propagating fatigue crack

The coating cracks initiate at nearly the same time in the early stage of the fatigue process, and it is necessary to consider the interaction of the cracks near the interface. For the two coplanar semi-elliptical surface flaws with the same dimensions in a finite thickness plate subjected to tension loading, the interaction effects between the stress-strain fields associated with both cracks (and their corresponding SIF values) mainly depend on the relative distance between them and the relative crack depth [34]. As shown in **Fig. 9(c)**, if the surface cracks of the coatings initiated at a relatively short distance from each other, the distance between the micro-cracks induced by the coating cracking on the substrate surface is also relatively short. As a matter of fact, the cracks could interact and give rise to stress intensity factor values higher than those experienced by single cracks [36]. Thus, the two substrate micro-cracks tend to coalesce, and then the coalesced crack propagates into the bulk material, as shown schematically in **Fig. 9(d)**.

The stress intensity factor of the coalesced crack is higher than of the single micro-cracks, so the coalesced crack propagates rapidly and becomes the main fatigue crack, causing the final material failure, while the single micro-cracks induced by the coating cracking, relatively far away from other micro-cracks, become the non-propagation fatigue cracks observed in **Fig. 6**.

4.3. Coating thickness effects on the fatigue limit

Due to the poor plastic deformation capacity compared with ductile substrate TC4, the cracking of brittle coatings happened in the early period of the fatigue process, and enhanced stress concentration [37] occurred at the crack tip of the micro-cracks on the substrate surface, accelerating the fatigue crack propagation process in the substrate.

As shown schematically in **Fig. 10**, we assume the coating crack is of the U-shape, the cracking direction is perpendicular to the loading direction, the depth of the crack (h) is the thickness of the coating, and the curvature radius (ρ) is equal to one unit length. The stress concentration factor α_σ is:

$$\alpha_\sigma = \frac{\sigma_{max}}{\sigma_n} = 1 + 2\sqrt{\frac{h}{\rho}} \tag{7}$$

The calculated α_σ for CrAlN, CrAlN×2 and TiN coatings, whose thickness is 4.5 μm, 9 μm, and 10 μm, respectively, is 5.24, 7 and 7.32.

Once the coatings cracking happened, the cracks propagate to the interface immediately with an extremely high speed, and the high-stress concentration level increased the effective stress applied on the substrate material under the coating cracks. According to equation (1), the stress intensity factor is directly proportional to the effective stress. Thus, the ΔK of the CrAlN×2 and TiN coatings are similar and higher than the CrAlN coating.

According to the above illustration, when the coatings' mechanical properties are similar

and adhesion is strong enough, the fatigue life of coated TC4 is determined by the coating thickness. This conclusion can be verified by the fatigue results of CrAlN, CrAlN×2 and TiN coated TC4 samples, shown in **Fig. 4**. The stress concentration factors of the coatings after the coating cracking happened (α_σ) are CrAlN< CrAlN×2< TiN, and the cycles to failure under 350 MPa applied maximum stress of CrAlN×2 and TiN samples are similar and lower than for the CrAlN samples. Thus, the larger the film thickness, the higher α_σ and the lower N_f of the coated sample under the same stress conditions, only in the premise that the fatigue cracks initiation effect of the coatings is similar.

5. Conclusions

Low-stress level tension-tension fatigue tests were performed on the TC4 alloy and coated samples. The coating gives a rise to a significant decrease in fatigue behavior. The fatigue limit of TC4 was between 510 and 530 MPa, and that of the samples with 4.5 μm thick CrAlN coating was between 315 and 330 MPa. The coatings prevented the deformation of TC4 samples at the beginning of the fatigue process before the coating cracking occurred, and the coating cracking can promote the elongation of the tested samples.

Normally, the fatigue cracks initiation mechanism is totally different for the coated and uncoated materials, and the coating cracking-induced low cyclic stress substrate damage model was proposed to illustrate the fatigue crack initiation mechanism in coated material. The fatigue crack initiation process for coated TC4 is substituted by the micro-cracks on the substrate surface induced by coating cracking, and there is obvious crack propagation path from the coating-substrate interface into the substrate on the fracture surface. On the other hand, the two micro-cracks, which are relatively close, tend to coalesce and propagate much easier, thus the single ones become the non-propagating fatigue cracks observed on the cross-section.

Serious stress concentration happened straight after the coating cracking, so if the coatings' mechanical properties are similar and the adhesion is strong enough, that is the effects on the fatigue initiation process are similar, the film thickness would have a significant influence on the fatigue life of the coated material.

Acknowledgments

This work was supported by the National Natural Science Foundation of China (51771025), the Beijing Nova Program (Z171100001117075) and the Fundamental Research Funds for the Central Universities (FRF-TP-17-002C1). AAV acknowledges support from the National Science Foundation (IRES 1358088).

References

[1] Baptista CARP, Barboza MJR, Adib AML, Andrade M, Otani C, Reis DAP. High temperature cyclic pressurization of titanium ducts for use in aircraft pneumatic systems. Materials & Design 2009;30:1503-10.

[2] Mughrabi H. On 'multi-stage' fatigue life diagrams and the relevant life-controlling mechanisms in ultrahigh-cycle fatigue. Fatigue & Fracture of Engineering Materials & Structures 2002;25:755-64.

[3] Saini BS, Gupta VK. Effect of WC/C PVD coating on fatigue behaviour of case carburized SAE8620 steel. Surface and Coatings Technology 2010;205:511-8.

[4] Hotta S, Itou Y, Saruki K, Arai T. Fatigue strength at a number of cycles of thin hard coated steels with quench-hardened substrates. Surface and Coatings Technology 1995;73:5-13.

[5] Ferreira JAM, Costa JDM, Lapa V. Fatigue behaviour of 42Cr Mo4 steel with PVD coatings. International Journal of Fatigue 1997;19:293-9.

[6] Puchi-Cabrera ES, Staia MH, Ochoa-Pérez EA, Teer DG, Santana-Méndez YY, La Barbera-Sosa JG, et al. Fatigue behavior of a 316L stainless steel coated with a DLC film deposited by PVD magnetron sputter ion plating. Materials Science and Engineering: A 2010;527:498-508.

[7] Costa MYP, Venditti MLR, Cioffi MOH, Voorwald HJC, Guimarães VA, Ruas R. Fatigue behavior of PVD coated Ti–6Al–4V alloy. International Journal of Fatigue 2011;33:759-65.

[8] Costa MYP, Cioffi MOH, Venditti MLR, Voorwald HJC. Fatigue fracture behavior of Ti-6Al-4V PVD coated. Procedia Engineering 2010;2:1859-64.

[9] Hong Y, Lei Z, Sun C, Zhao A. Propensities of crack interior initiation and early growth for very-high-cycle fatigue of high strength steels. International Journal of Fatigue 2014;58:144-51.

[10] Spriestersbach D, Brodyanski A, Lösch J, Kopnarski M, Kerscher E. Very high cycle fatigue of high-strength steels: Crack initiation by FGA formation investigated at artificial defects. Procedia Structural Integrity 2016;2:1101-8.

[11] Murakam Y, Nomoto T, Ueda T. Factors influencing the mechanism of superlong fatigue failure in steels. Fatigue & Fracture of Engineering Materials & Structures 1999;22:581-90.

[12] Shanyavskiy AA. Mechanisms and modeling of subsurface fatigue cracking in metals.

Engineering Fracture Mechanics 2013;110:350-63.

[13] Heinz S, Eifler D. Crack initiation mechanisms of Ti6Al4V in the very high cycle fatigue regime. International Journal of Fatigue 2016;93:301-8.

[14] Umezawa O, Nagai K. Deformation structure and subsurface fatigue crack generation in austenitic steels at low temperature. Metallurgical and Materials Transactions A 1998;29:809-22.

[15] Joseph S, Lindley TC, Dye D. Dislocation interactions and crack nucleation in a fatigued near-alpha titanium alloy. International Journal of Plasticity 2018.

[16] Heinz S, Balle F, Wagner G, Eifler D. Analysis of fatigue properties and failure mechanisms of Ti6Al4V in the very high cycle fatigue regime using ultrasonic technology and 3D laser scanning vibrometry. Ultrasonics 2013;53:1433-40.

[17] Joseph S, Bantounas I, Lindley TC, Dye D. Slip transfer and deformation structures resulting from the low cycle fatigue of near-alpha titanium alloy Ti-6242Si. International Journal of Plasticity 2018;100:90-103.

[18] Chai G. The formation of subsurface non-defect fatigue crack origins. International Journal of Fatigue 2006;28:1533-9.

[19] Su H, Liu X, Sun C, Hong Y. Nanograin layer formation at crack initiation region for very-high-cycle fatigue of a Ti-6Al-4V alloy. Fatigue & Fracture of Engineering Materials & Structures 2017;40:979-93.

[20] Yin D, Liu H, Chen Y, Yi D, Wang B, Wang B, et al. Effect of grain size on fatigue-crack growth in 2524 aluminium alloy. International Journal of Fatigue 2016;84:9-16.

[21] Trudel A, Lévesque M, Brochu M. Microstructural effects on the fatigue crack growth resistance of a stainless steel CA6NM weld. Engineering Fracture Mechanics 2014;115:60-72.

[22] Li L, Zhang Z, Shen G. The Effect of Grain Size on Fatigue Crack Propagation in Commercial Pure Titanium Investigated by Acoustic Emission. Journal of Materials Engineering and Performance 2015;24:2720-9.

[23] Xu T, Feng Y, Song S, Wang D. Fatigue crack propagation behaviour of steels with different microstructures. Materials Science and Engineering: A 2012;551:110-5.

[24] Blochwitz C, Richter R. Plastic strain amplitude dependent surface path of microstructurally short fatigue cracks in face-centred cubic metals. Materials Science and Engineering: A 1999;267:120-9.

[25] Zhao YX, Yang B, Feng MF, Wang H. Probabilistic fatigue S–N curves including the super-long life regime of a railway axle steel. International Journal of Fatigue 2009;31:1550-8.

[26] Brame DR, Evans T. Deformation of thin films on solid substrates. Philosophical Magazine 1958;3:971-86.

[27] Zhang T-Y, Qian C-F, Wang T, Tong P. Interaction of an edge dislocation with a thin-film-covered crack. International Journal of Solids and Structures 2000;37:5465-92.

[28] Zhang T-Y, Qian C-F. Interaction of a screw dislocation with a thin-film-covered mode III crack. Acta Materialia 1996;44:4513-20.

[29] Martin DM, McGee TD. The interaction of dislocations and boundaries. Acta Metallurgica 1969;17:929-32.

[30] Tanaka K, Akiniwa Y. Fatigue crack propagation behaviour derived from S–N data in very high cycle regime. Fatigue & Fracture of Engineering Materials & Structures 2002;25:775-84.

[31] Murakami Y, Kodama S, Konuma S. Quantitative evaluation of effects of non-metallic inclusions on fatigue strength of high strength steels. I: Basic fatigue mechanism and evaluation of correlation between the fatigue fracture stress and the size and location of non-metallic inclusions. International Journal of Fatigue 1989;11:291-8.

[32] Xi Y, Bai Y, Gao K, Pang X, Yang H, Yan L, et al. In-situ stress gradient evolution and texture-dependent fracture of brittle ceramic thin films under external load. Ceramics International 2018;44:8176-83.

[33] Wang A-N, Yu G-P, Huang J-H. Fracture toughness measurement on TiN hard coatings using internal energy induced cracking. Surface and Coatings Technology 2014;239:20-7.

[34] Shi K, Cai L, Chen L, Bao C. A theoretical model of semi-elliptic surface crack growth. Chinese Journal of Aeronautics 2014;27:730-4.

[35] Carpinteri A, Brighenti R, Vantadori S. A numerical analysis on the interaction of twin coplanar flaws. Engineering Fracture Mechanics 2004;71:485-99.

[36] Carpinteri A, Brighenti R, Vantadori S. A numerical analysis on the interaction of twin coplanar flaws. Engineering Fracture Mechanics 2004;71:485-99.

[37] Ding F, Feng M, Jiang Y. Modeling of fatigue crack growth from a notch. International Journal of Plasticity 2007;23:1167-88.

Figure Captions

Fig. 1. Elastic modulus and hardness of the tested materials.

Fig. 2. Specimen dimensions in mm used in fatigue tests.

Fig. 3. Fatigue test results in terms of the S-N data for the TC4 substrate and coated specimens. (Crosses mean over 10^7 fatigue cycles without failure.)

Fig. 4. Optical images of the fatigue crack surface morphology and displacement-number of cycles relationship for TC4 and coated samples during fatigue tests: (a) TC4, 515 MPa; (b) CrAlN, 565 MPa; (c) CrAlN×2, 350 MPa; (d) TiN, 300 MPa.

Fig. 5. Fig. 5. Schematic diagram of the deformation mechanism of TC4 and coated TC4 material: (a) dislocations pile-up at the phase boundary of primary α and laminar β phases at the subsurface of TC4; (b) the dislocation crosses the grain boundary and piles-up at the specimen's surface; (c) glide step appeared on the specimen's surface and the plastic elongation of TC4 specimen through sliding is denoted as Δl; (d) dislocations pile-up at the coating-substrate interface and no slip deformation occurs; (e) the coating cracking caused the fatigue crack initiation and the crack opening displacement is regarded as the plastic elongation of the coated specimen, denoted as $\Delta l'$.

Fig. 6. SEM micrographs of: (a) crack tip cross-section and (b) non-propagating cracks in CrAlN coated sample surface, tested under 500 MPa and stopped manually when the cracks propagated to about 500 μm; (c) a sketch of crack tip section sampling location.

Fig. 7. Detailed morphology of fatigue crack initiation region in: (a) TC4, (b) CrAlN, (c) CrAlN×2 and (d) TiN coated samples.

Fig. 8. Fatigue crack initiation process in coated TC4: (a) coating fatigue cracking initiated at the middle of the hard coating; (b) substrate damage (micro-cracks) induced by coating cracking; (c) the micro-cracks propagated under cyclic loading; (d) the main fatigue crack.

Fig. 9. Schematic diagram of coating cracking-induced low cyclic stress substrate damage model: (a) coating crack propagated to the interface; (b) substrate surface damage induced by coating cracking; (c) two cracks within a relatively short distance; (d) the coalesced crack propagates into the bulk material.

Fig. 10. Schematic diagram of the coating crack tip at the interface.

Fig. 1

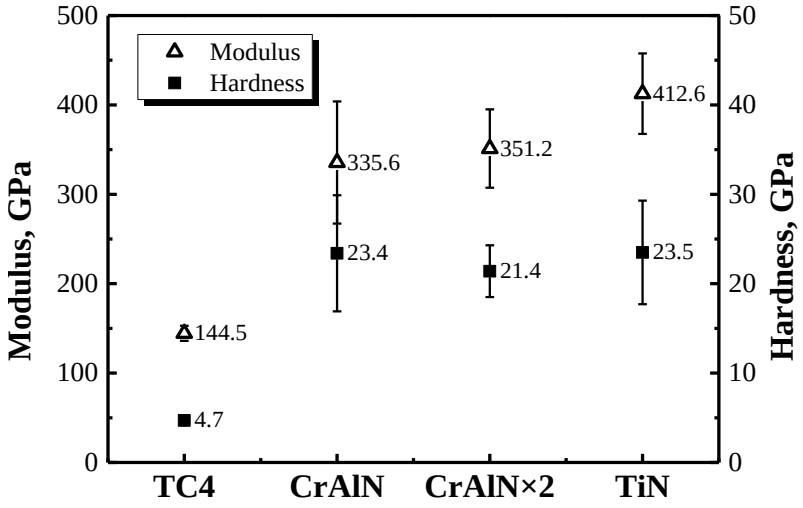
Modulus
Hardness
Modulus, GPa
Hardness, GPa
500
400
300
200
100
0
50
40
30
20
10
0
144.5
4.7
335.6
23.4
351.2
21.4
412.6
23.5
TC4
CrAlN
CrAlN×2
TiN

Fig. 2

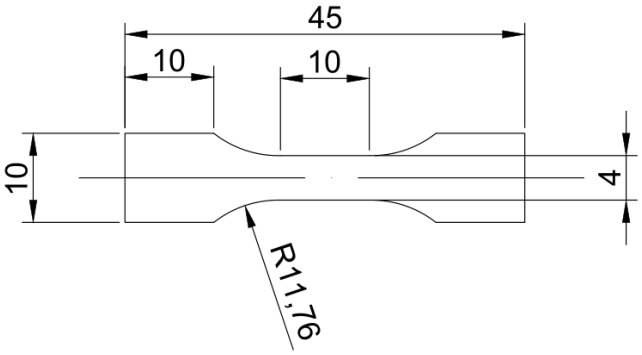

Fig. 3

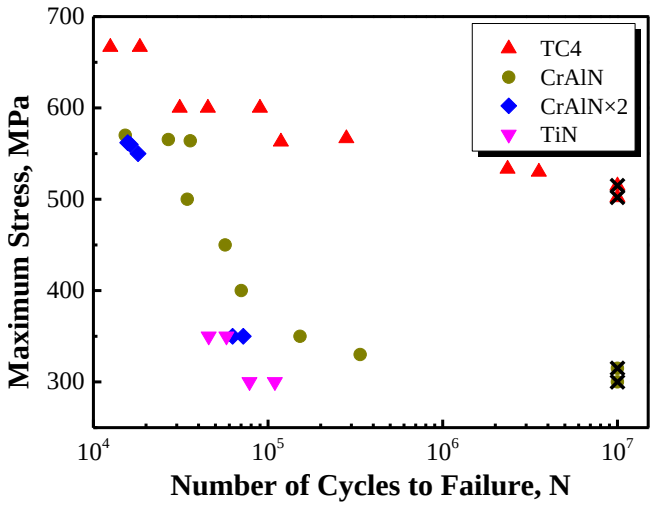
Maximum Stress, MPa
700
600
500
400
300
10^4
10^5
10^6
10^7
Number of Cycles to Failure, N
TC4
CrAlN
CrAlN×2
TiN

Fig. 4

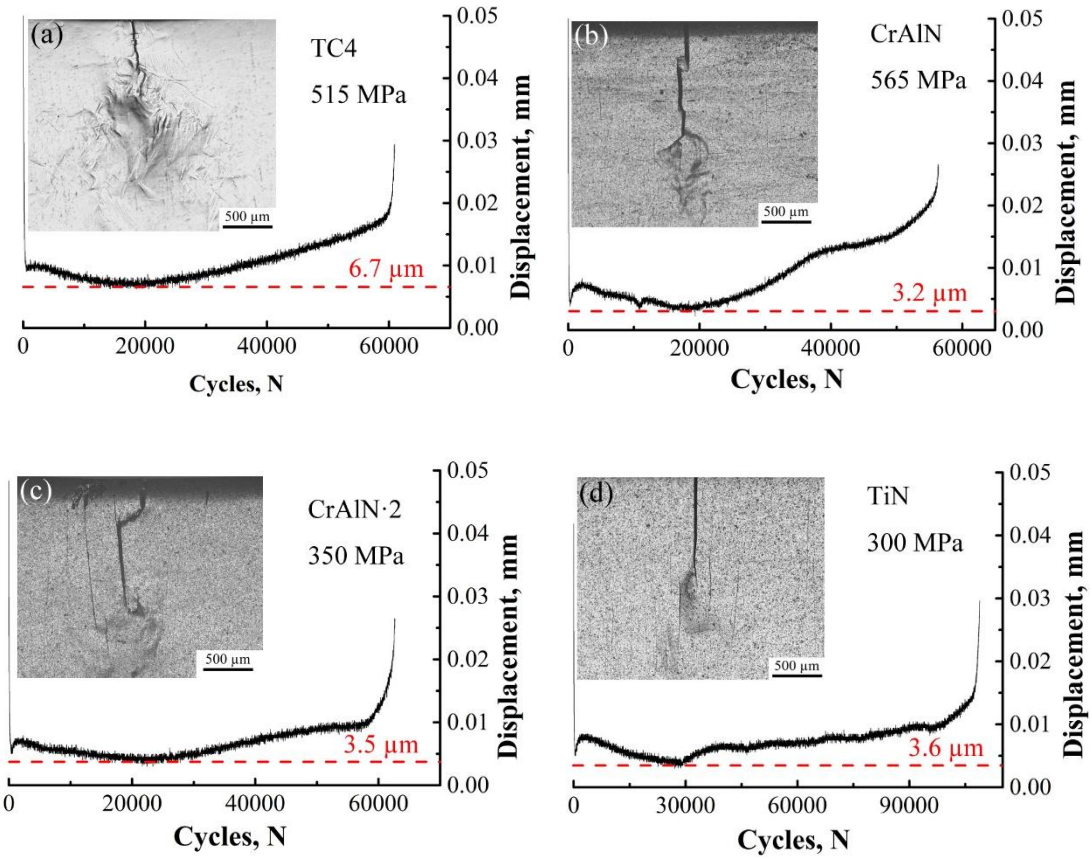
(a)
TC4
515 MPa
500 μm
6.7 μm
0
20000
40000
60000
Cycles, N
0.00
0.01
0.02
0.03
0.04
0.05
Displacement, mm
(b)
CrAlN
565 MPa
500 μm
3.2 μm
0
20000
40000
60000
Cycles, N
0.00
0.01
0.02
0.03
0.04
0.05
Displacement, mm
(c)
CrAlN·2
350 MPa
500 μm
3.5 μm
0
20000
40000
60000
Cycles, N
0.00
0.01
0.02
0.03
0.04
0.05
Displacement, mm
(d)
TiN
300 MPa
500 μm
3.6 μm
0
30000
60000
90000
Cycles, N
0.00
0.01
0.02
0.03
0.04
0.05
Displacement, mm

Fig. 5

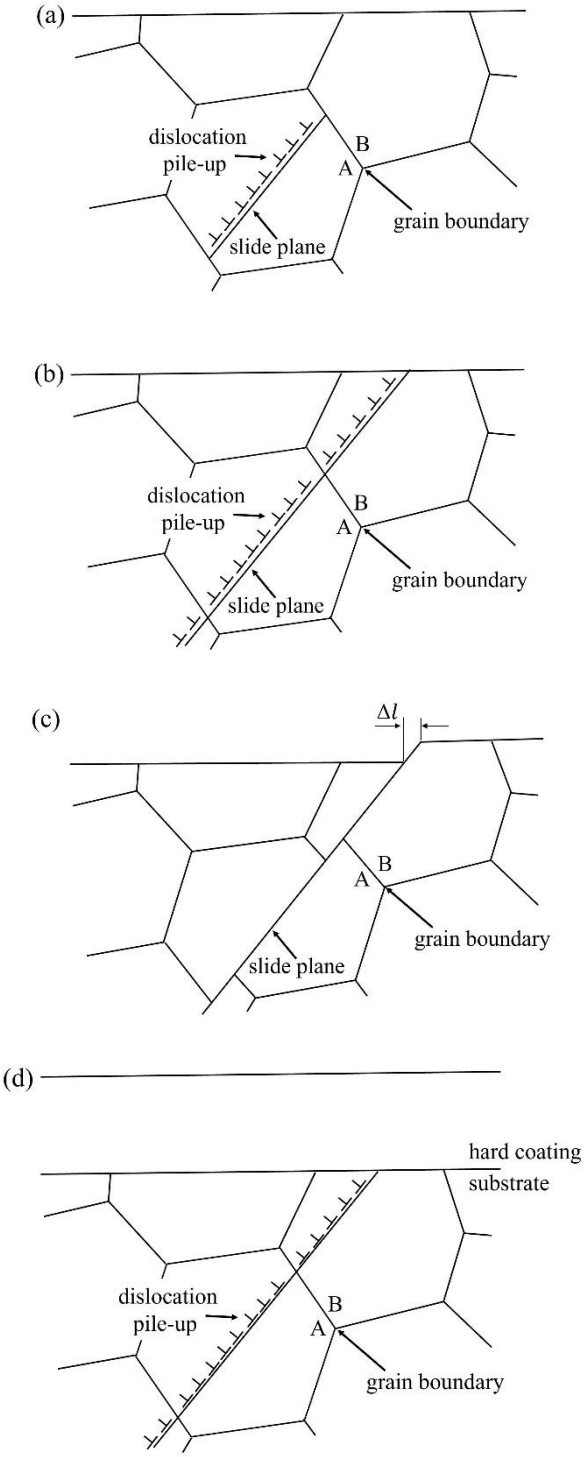
(a)
dislocation
pile-up
B
A
grain boundary
slide plane
(b)
dislocation
pile-up
B
A
grain boundary
slide plane
(c)
Δl
B
A
grain boundary
slide plane
(d)
hard coating
substrate
dislocation
pile-up
B
A
grain boundary

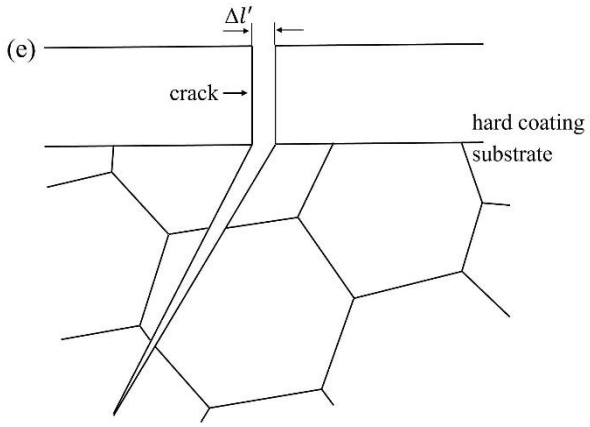
(e)
$\Delta l'$
crack
hard coating
substrate

Fig. 6

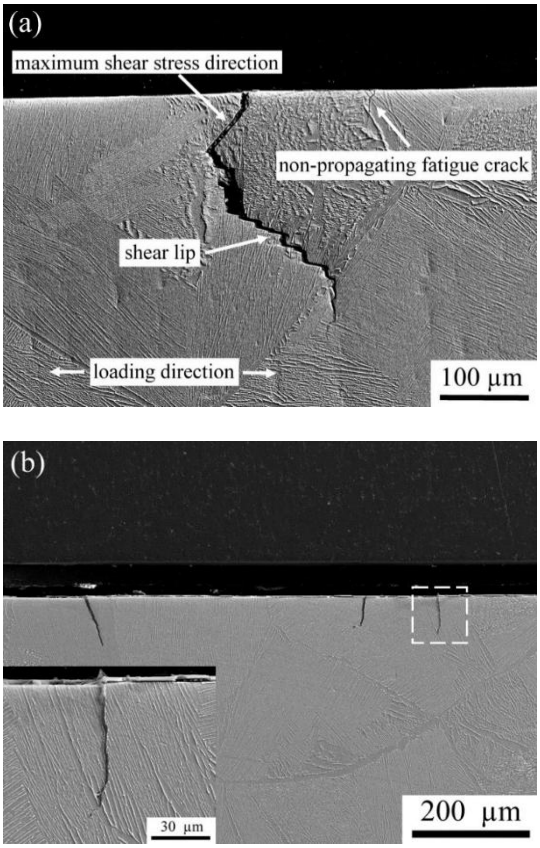
(a)
maximum shear stress direction
non-propagating fatigue crack
shear lip
loading direction
100 μm
(b)
30 μm
200 μm
(c)
crack tip section sampling location
coating cracks on surface
lightning-like shape main crack
coating
substrate
main fatigue crack in substrate

Fig. 7

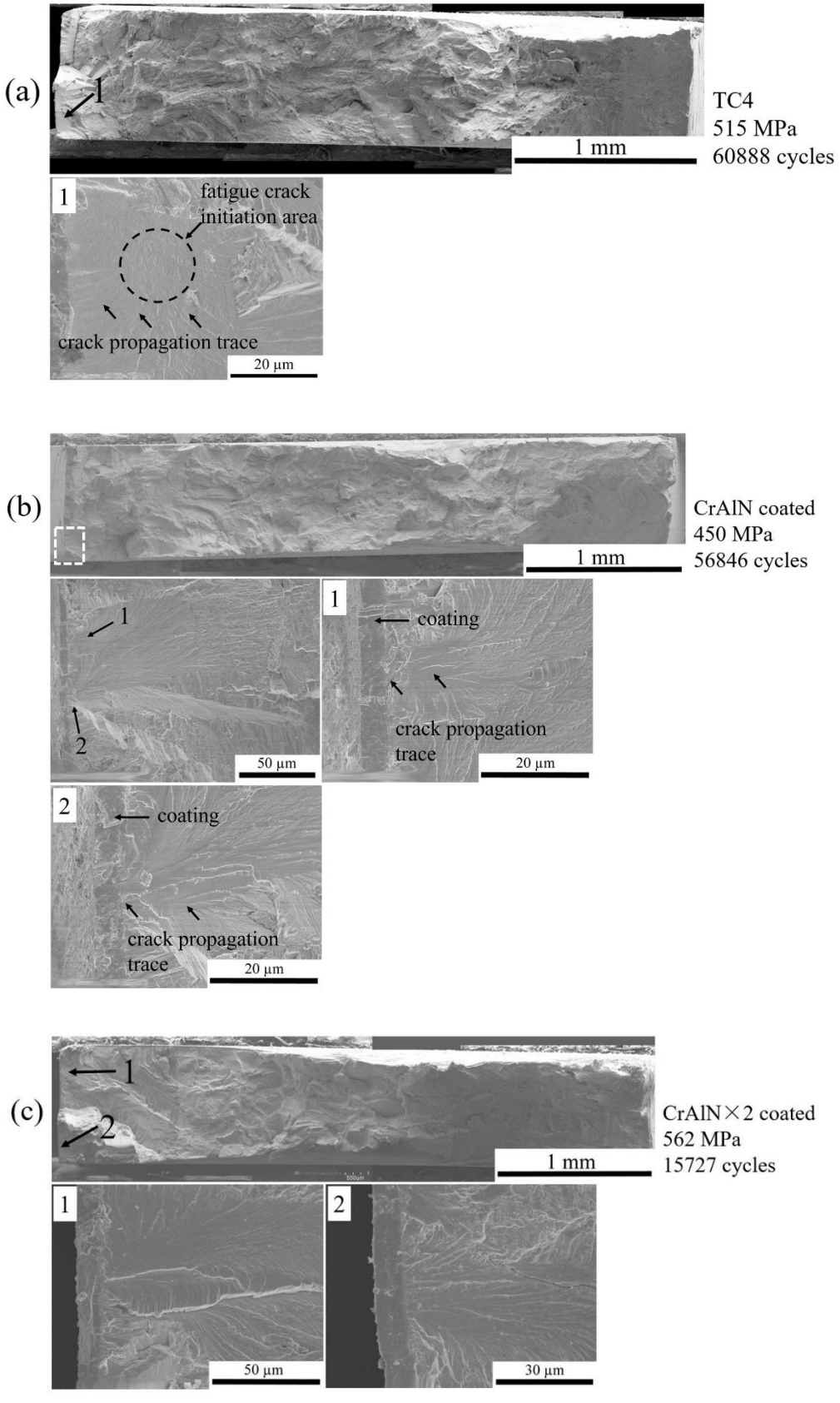
(a)
1
1 mm
TC4
515 MPa
60888 cycles
1
fatigue crack initiation area
crack propagation trace
20 μm
(b)
1 mm
CrAlN coated
450 MPa
56846 cycles
1
2
50 μm
1
coating
crack propagation trace
20 μm
2
coating
crack propagation trace
20 μm
(c)
1
2
1 mm
CrAlN×2 coated
562 MPa
15727 cycles
1
50 μm
2
30 μm

(d)

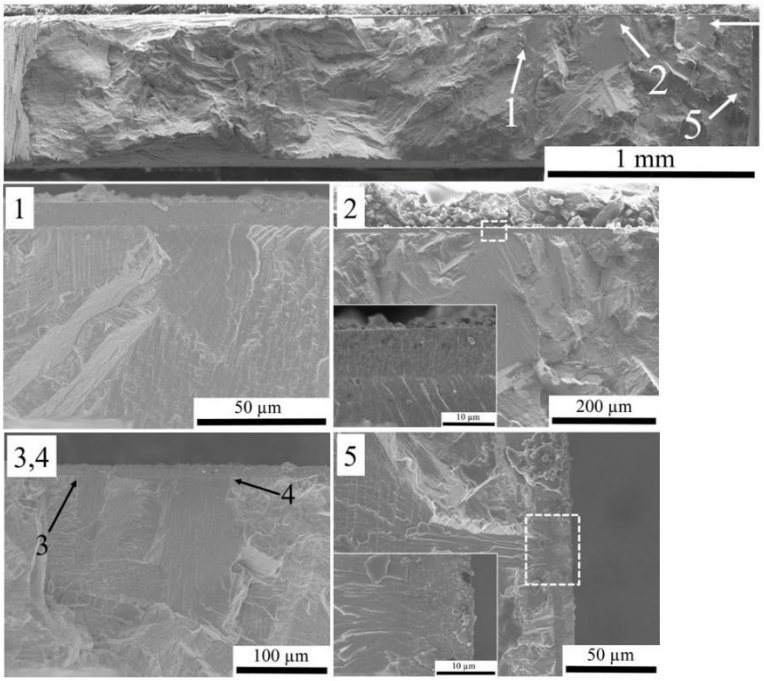
3,4
1
2
5
1 mm
TiN coated
300 MPa
109338 cycles
1
50 µm
2
200 µm
10 µm
3,4
3
4
100 µm
5
50 µm
10 µm

Fig. 8

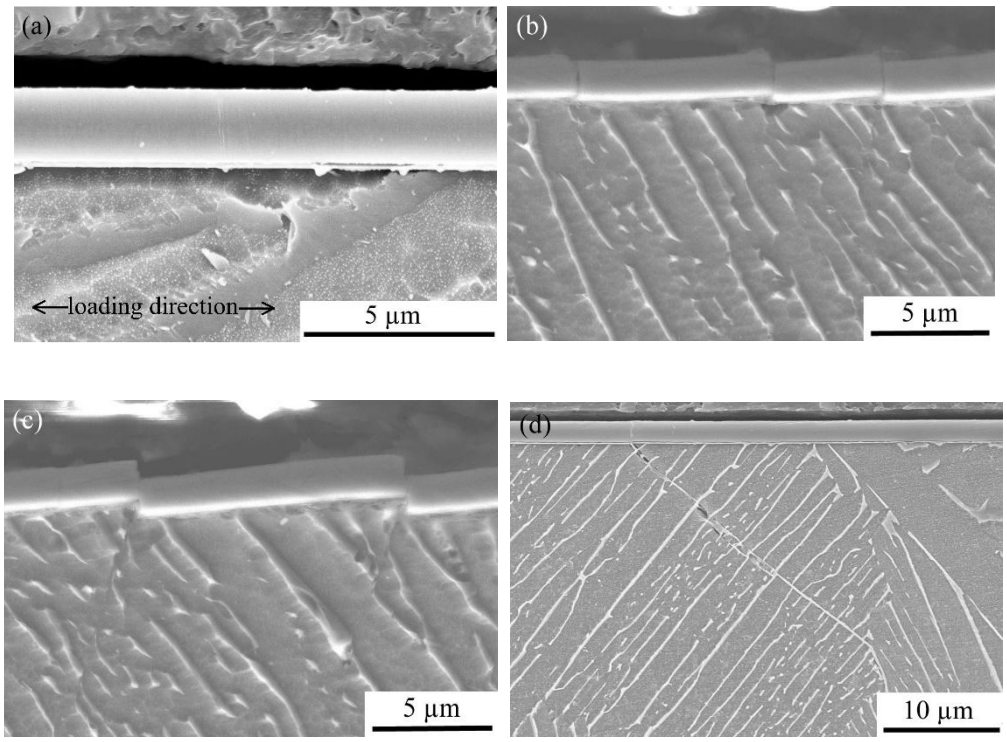

Fig. 9

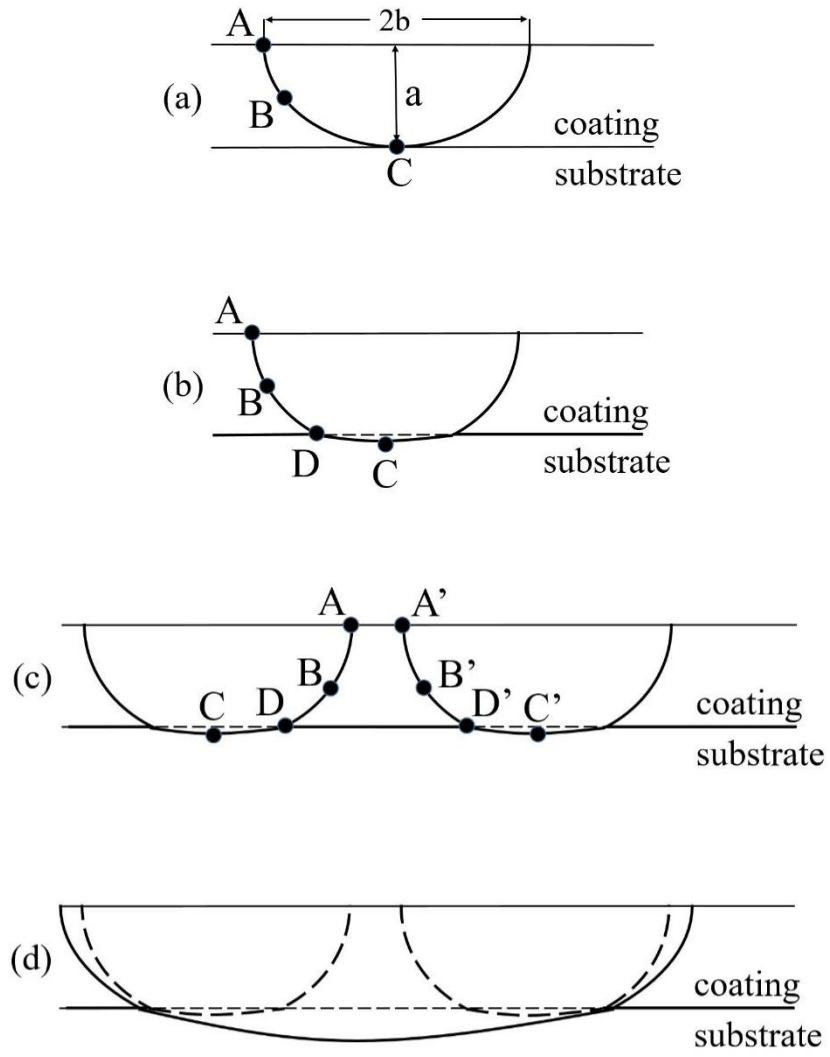
A
2b
(a)
B
a
coating
C
substrate
A
(b)
B
coating
D
C
substrate
A
A'
(c)
B
B'
C
D
D'
C'
coating
substrate
(d)
coating
substrate

Fig. 10

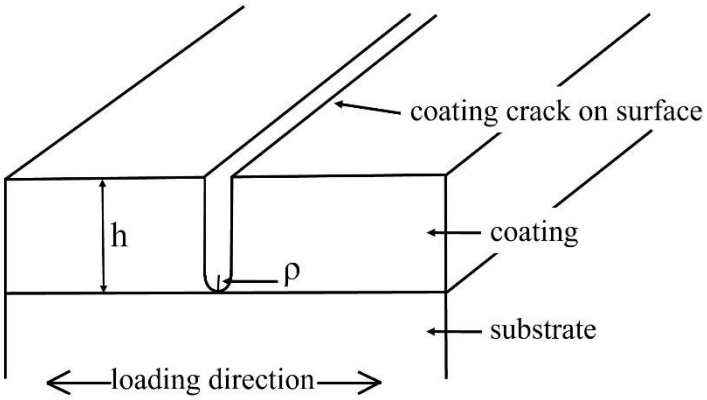
coating crack on surface
h
ρ
coating
substrate
loading direction